JCI The Journal of Clinical Investigation

An attenuated lymphocytic choriomeningitis virus vector enhances tumor control in mice partly via IFN-I

Young Rock Chung, … , Slim Fourati, Pablo Penaloza-MacMaster

J Clin Invest. 2024. https://doi.org/10.1172/JCI178945.

Research In-Press Preview **Immunology**

Viral vectors are being used for the treatment of cancer. Yet their efficacy varies among tumors and their use poses challenges in immunosuppressed patients, underscoring the need for alternatives. We report striking antitumoral effects by a nonlytic viral vector based on attenuated lymphocytic choriomeningitis virus (r3LCMV). We show in multiple tumor models that injection of tumor-bearing mice with this vector results in improved tumor control and survival. Importantly, r3LCMV improved tumor control in immunodeficient *Rag1*$^{-/-}$ mice and *MyD88*$^{-/-}$ mice, suggesting that multiple pathways contributed to the antitumoral effects. The antitumoral effects of r3LCMV were also observed when this vector was administered several weeks before tumor challenges, suggesting the induction of trained immunity. Single cell RNA-Seq analyses, antibody blockade experiments, and KO models revealed a critical role for host-intrinsic IFN-I in the antitumoral efficacy of r3LCMV vectors. Collectively, these data demonstrate potent antitumoral effects by r3LCMV vectors and unveil multiple mechanisms underlying their antitumoral efficacy.

An attenuated lymphocytic choriomeningitis virus vector enhances tumor control in mice partly via IFN-I

Young Rock ChungΨ[1], Bakare AwakoaiyeΨ[1], Tanushree Dangi[1], Nahid Irani[1], Slim Fourati[2], Pablo Penaloza-MacMaster*[1]

[1]Department of Microbiology-Immunology, Feinberg School of Medicine, Northwestern University, Chicago, IL 60611, USA. [2]Department of Medicine, Division of Allergy and Immunology, Feinberg School of Medicine and Center for Human Immunobiology, Northwestern University, Chicago, IL 60611, USA.

Ψ **Equal contribution**

*** Correspondence and Lead contact:**

Pablo Penaloza-MacMaster (ppm@northwestern.edu)

303 E Chicago Ave, Tarry 6-729, Chicago, IL, 60611, U.S.A.

Phone: 312-503-0357

Abstract:

Viral vectors are being used for the treatment of cancer. Yet their efficacy varies among tumors and their use poses challenges in immunosuppressed patients, underscoring the need for alternatives. We report striking antitumoral effects by a nonlytic viral vector based on attenuated lymphocytic choriomeningitis virus (r3LCMV). We show in multiple tumor models that injection of tumor-bearing mice with this vector results in improved tumor control and survival. Importantly, r3LCMV improved tumor control in immunodeficient *Rag1*-/- mice and *MyD88*-/- mice, suggesting that multiple pathways contributed to the antitumoral effects. The antitumoral effects of r3LCMV were also observed when this vector was administered several weeks before tumor challenges, suggesting the induction of trained immunity. Single cell RNA-Seq analyses, antibody blockade experiments, and KO models revealed a critical role for host-intrinsic IFN-I in the antitumoral efficacy of r3LCMV vectors. Collectively, these data demonstrate potent antitumoral effects by r3LCMV vectors and unveil multiple mechanisms underlying their antitumoral efficacy.

Introduction:

Cancer is linked to immunosuppression, which inhibits the ability of the immune system to clear tumor cells. A specific challenge in cancer immunotherapies is the presence of "cold tumors," where the immune system fails to respond to tumor cells. This process can be triggered by the recruitment of regulatory T cells to the tumor microenvironment, as well as by the upregulation of inhibitory receptors such as PD-1 and CTLA-4, among many other factors. While immune checkpoint therapy can partially revert immunosuppression and result in effective tumor control, only ~30% of patients respond, highlighting the need for alternative immunotherapies. Viruses have emerged as attractive therapies to overcome immunosuppression during cancer. In particular, oncolytic viruses that preferentially infect and replicate in tumor cells have been extensively explored for cancer immunotherapy (1). Currently, an oncolytic virus (talimogene laherparepvec, T-VEC) is approved for melanoma patients (2). Although this vector can be effective in some patients with melanoma, adverse effects have been reported following the use of this replicating lytic virus, and not all patients respond. Due to safety concerns, immunocompromised patients are typically excluded from receiving this replicating lytic viral therapy, motivating the development of alternative viral vectors for cancer immunotherapy.

In this study, we explored a non-lytic virus, lymphocytic choriomeningitis virus (LCMV), as a cancer immunotherapy. LCMV can be engineered to serve as a replication-attenuated vector that can deliver foreign antigens to the immune system (3, 4). Prior

studies have shown that immunization of mice with attenuated LCMV vectors expressing tumor antigens improves tumor control and there is an ongoing trial evaluating the efficacy of attenuated LCMV vectors expressing HPV antigens in patients with HPV16+ metastatic head and neck carcinoma (#NCT04180215) (5-7). The use of viral vectors expressing a cargo of tumor antigens requires knowledge of specific tumor antigens, which may differ depending on the patient and the type of tumor. In this study we interrogated whether replication-attenuated r3LCMV vectors that do not express any tumor antigen provide antitumor protection. Using multiple tumor models, we show that injection of tumor-bearing mice with r3LCMV vectors results in improved tumor control and prolonged survival. Moreover, we demonstrate that the antitumoral effects of r3LCMV are partly dependent on the IFN-I pathway.

Results

Comparative analyses of antitumoral effects by replicating and non-replicating LCMV vectors.

Due to their high immunogenicity, LCMV vectors have been explored as vaccine candidates for various diseases (8-10). In these prior studies, LCMV vectors have been genetically modified to include a foreign antigen to prime antigen-specific immune responses. In our study, however, we tested whether an LCMV vector that does not express any tumor antigen can confer “bystander” protection against tumor challenges in mice. We first challenged C57BL/6 mice with 10^6 B16 melanoma cells and at day 5 post-challenge, we treated tumor-bearing mice intratumorally with $2x10^5$ focus forming units (FFU) of a replication-attenuated LCMV vector (r3LCMV) (**Figure 1A**). At day 4 post-treatment, we harvested tumors and measured viral antigen by immunofluorescence. Viral antigen was highly co-localized with F4/80+ cells in mice treated with r3LCMV, suggesting that macrophages were preferentially infected with r3LCMV (**Figure 1B**). We also interrogated whether r3LCMV could replicate in B16 melanoma cells. To answer this question, we incubated B16 melanoma cells for 48 hr with r3LCMV vectors expressing a reporter green fluorescent protein (GFP) at a multiplicity of infection (MOI) of 0.1, and then we measured viral antigen by immunofluorescence. The r3LCMV vector was able to infect B16 melanoma cells in vitro, consistent with a prior study (11); for comparison, we included a non-replicating (rLCMV) vector, which was able to enter melanoma cells, but resulted in lower antigen levels (**Supplemental Figure 1, A-B**).

We also evaluated whether intratumoral treatment with r3LCMV improves tumor control. Interestingly, treatment of tumor-bearing mice with r3LCMV induced a significant improvement in tumor control (**Figure 1C**) associated with generation of virus-specific CD8 T cell responses (**Figure 1D**). To determine whether the antimoral effect of the LCMV vector was affected by the ability of the virus to replicate, we injected B16 melanoma-bearing mice with replicating or non-replicating LCMV vectors (both were attenuated relative to wild-type LCMV). We utilized the bisegmented rLCMV vector that can enter cells and express viral proteins but cannot induce a second round of infection due to a genetic absence of the glycoprotein (GP) gene, the viral protein that mediates viral entry. During the in vitro production of this bisegmented rLCMV vector, the GP is only provided *in trans* in the producer cells to allow entry of the vector into host cells, but progeny virions are unable to form infectious progeny virions due to genetic lack of the GP. On the other hand, the r3LCMV vector expresses GP *in cis*, allowing it to undergo several replication cycles until it is eliminated by the host's immune response , but it is still significantly attenuated and does not replicate to wild-type levels (12) (**Supplemental Figure 1C**). Interestingly, the replicating (r3LCMV) vector resulted in a superior antitumoral effect relative to non-replicating (rLCMV) vector (**Figure 2, A-D**).

Intratumoral r3LCMV therapy also induced potent antitumoral effects in other tumor models, such as the MC38 colon adenocarcinoma (**Figure 2, E-F**), and in mice with different genetic backgrounds (**Figure 2, G-H**), suggesting a generalizable antitumor effect independent of the major histocompatibility complex (MHC) haplotype. To a lesser extent, a replicating vesicular stomatitis virus (VSV), and the replicating yellow fever virus

(YFV-17D) vaccine also induced antitumoral effects (**Figure 2, I-L**), suggesting that replicating viral vectors exert superior antitumoral effects than non-replicating viral vectors. We also tested antitumoral effects on distal tumors, known as abscopal effect. To test this, we injected both flanks of the mice with B16 melanoma cells, followed by intratumoral r3LCMV injection in the right tumor only. Interestingly, r3LCMV also induced partial regression of the contralateral (left) tumor (**Supplemental Figure 2**), demonstrating the induction of abscopal effect. Further, we compared tumor control elicited by r3LCMV versus PD-L1 blockade (**Supplemental Figure 3A**). Treatment with r3LCMV alone resulted in significantly superior antitumoral control relative to PD-L1 blockade alone, and there was a pattern of improved survival in mice that received combined treatment, although the difference was not statistically significant (**Supplemental Figure 3, B-C**).

In addition, we observed that treatment of tumor-bearing mice with r3LCMV induced a significant reduction of systemic and tumor-draining lymph node regulatory T cells (Tregs) after a week of treatment (**Supplemental Figure 4, A-C**). Treg depletion has been shown to improve tumor control (13), so we examined whether their depletion could synergize with r3LCMV treatment. We utilized FoxP3-DTR mice, which allow for depletion of Tregs upon diphtheria toxin administration (14). Our data show that Treg depletion combined with r3LCMV treatment results in more potent antitumoral control, relative to Treg depletion alone (**Supplemental Figure 4, D-E**).

Role for antigen presentation, costimulation, and T cells.

T cells are thought to be critical for the control of tumors, and their activation is dependent on MHC antigen presentation and costimulation. We first examined the role of antigen presentation by challenging mice with β2-microglubulin KO (*B2m* -/-) B16 melanoma cells, which are unable to present antigen to CD8 T cells (15). β *B2m* -/- B16 tumor-bearing mice were then treated with PBS or r3LCMV and tumor control was measured. Interestingly, *B2m* -/- B16 tumor-bearing mice treated with r3LCMV showed improved tumor control relative to control treated mice, suggesting that antigen presentation via MHC was not completely required for the antitumoral effect (**Figure 3, A-C**).

We then evaluated whether the r3LCMV treatment improves tumor-specific T cell responses, by challenging mice with B16 melanoma cells expressing ovalbumin (B16-OVA), and then measuring OVA-specific CD8 T cell responses by K^bSIINFEKL tetramer staining. The r3LCMV treatment did not improve tumor-specific (SIINFEKL-specific) CD8 T cell responses (**Figure 3, D-E**). We then measured costimulatory molecule expression on dendritic cells (DC) from tumor-draining lymph nodes following r3LCMV treatment, and we observed a significant increase in CD80 (B7.1) and CD86 (B7.2) molecule expression in mice that received r3LCMV treatment (**Figure 3F**), suggesting a role for B7 costimulation. However, blockade of B7.1 and B7.2 molecules did not abrogate the antitumoral effect of r3LCMV (**Figure 3, G-H**), suggesting that B7/CD28 costimulation was dispensable for the antitumoral effect of r3LCMV. We further examined the role for CD4 T cell responses by depleting these cells using depleting antibodies. CD4 T cell depletion did not impair the antitumoral effect of r3LCMV (**Figure 3H**).

Moreover, we performed CD8 T cell depletion experiments to evaluate whether CD8 T cells were mechanistically involved. CD8 T cell depletion did not significantly impact the antitumoral effect of r3LCMV (**Figure 3H**). These findings did not necessarily indicate that T cells are dispensable for the antitumoral effect of r3LCMV, since treatment with T cell depleting antibodies may not fully deplete all T cells in tissues. Thus, we utilized an adoptive CD8 T cell transfer model to more rigorously measure the contribution of virus-specific CD8 T cells in tumor control. We adoptively transferred TCR transgenic CD8 T cells recognizing the LCMV GP33-41 epitope (P14 cells) into recipient tumor-bearing OT-I mice, which contain only OVA-specific CD8 T cells. This adoptive transfer model allowed us to examine the contribution of virus-specific CD8 T cell activation in a "T cell-replete" environment. We used OT-I mice as recipients instead of *Rag1*-/- mice because transferring donor T cells into *Rag1*-/- mice would lead to rapid homeostatic proliferation of donor T cells (emptiness-induced proliferation) and other immune abnormalities caused by the absence of T cells and B cells (16). One day after P14 cell transfer, recipient mice were infected intratumorally with an LCMV variant lacking the GP33-41 epitope (LCMV ∆GP33) or a wild-type LCMV (Cl-13) to determine whether the activation of virus-specific CD8 T cells potentiates tumor control (**Figure 3I**). Both LCMV strains replicate at comparable levels and the only difference is a valine to alanine (V→A) escape mutation that destroys the GP33 epitope recognized by P14 cells (17). As expected, intratumoral treatment with the wild-type LCMV (but not the LCMV ∆GP33 variant) triggered robust P14 cell expansion in the tumor-bearing mice (**Figure 3J**). Interestingly, the mice that were infected with the wild-type LCMV (which showed robust P14

expansion) exhibited superior tumor control relative to the mice that were infected with the LCMV ∆GP33 variant **(Figure 3K**), suggesting that "bystander" activation of virus-specific CD8 T cells can facilitate tumor control in a host devoid of tumor-specific T cell responses. Collectively, these data using transgenic P14 cells suggested that the bystander activation of virus-specific T cells could potentiate tumor control, without the need for tumor-specific T cells.

r3LCMV improves tumor control in the absence of adaptive immunity.

To interrogate the role of adaptive immunity more rigorously, we challenged *Rag1*-/- mice with B16 tumor cells, followed by treatment with r3LCMV (**Figure 4A**). *Rag1*-/- mice are unable to generate mature T cells and B cells, leading to severe combined immunodeficiency. Interestingly, *Rag1*-/- mice also exhibited a significant improvement in tumor control after r3LCMV treatment, demonstrating that r3LCMV could also induce antitumoral effects in the absence of adaptive immunity (**Figure 4, B-C**). These data do not necessarily contradict our findings above using P14 cells. We reason that although virus-specific T cells can facilitate tumor control, they are not the only component of the immune response that is required for the antitumoral effect of r3LCMV. It is also important to mention that the surviving *Rag1*-/- mice that were treated with r3LCMV were unable to clear the vector due to lack of T cells (**Figure 4D**), but they appeared normal and without any signs of disease. We also examined whether the antitumoral effect of r3LCMV was dependent on IFNγ, also known as "adaptive interferon." IFNγ is expressed mostly by effector T cells and this cytokine is important for tumor control (18). To examine the role

of IFNγ on tumor cells, we challenged C57BL/6 mice with B16 melanoma cells lacking the IFNγ receptor (*Ifngr1*-/-). We then treated mice with PBS or r3LCMV to examine whether tumor control by r3LCMV therapy was dependent on tumor-intrinsic IFNγ signaling. Importantly, tumor control by r3LCMV was not dependent on tumor-intrinsic IFNγ signaling (**Supplemental Figure 5**), suggesting that tumor control by r3LCMV therapy was not dependent on tumor-intrinsic "adaptive" interferon signaling.

Single cell RNA-Seq (scRNA-Seq) analyses reveal a role for type I interferons.

We then performed gene expression analyses to understand the effects of r3LCMV on different cell subsets within the tumor microenvironment. We harvested tumors at day 4 post-treatment, followed by scRNA-Seq analyses. We observed differences in cell populations between the PBS and r3LCMV treated mice. Our single cell gene expression data show that r3LCMV induces changes in cell frequencies within the tumor microenvironment, including a significant influx of natural killer (NK) cells and macrophages (**Figure 5A**). LCMV viral reads were detected in r3LCMV treated mice, especially in DCs, macrophages, and tumor cells themselves (which harbored the L and S RNA segments from LCMV) (**Figure 5, A-B**). These gene expression data also show that r3LCMV induces several IFN-induced genes (ISG), including those coding for master transcription factor Irf7 and transcripts for the antiviral proteins Ifi3 and Isg15 (**Figure 5C**). ISG were significantly upregulated in immune cell subsets; but not in tumor cells when analyzed as a whole (when compounding uninfected and infected tumor cells) (**Figure 5D**). However, when we compared tumor cells containing viral transcripts to tumor cells

lacking viral transcripts in the r3LCMV treated mice, we observed significant upregulation of ISG only in tumor cells containing viral transcripts (**Figure 5E**). These data suggested a possible role for IFN-I in the antitumoral control elicited by r3LCMV.

We then validated the gene expression data at the protein level. IFN-I and interferon-induced cytokines were highly upregulated in the serum of mice treated with r3LCMV (**Figure 6A**), consistent with other studies examining cytokine responses with other LCMV vectors (7, 12). IFN-I levels were higher after treatment with the replicating vector (r3LCMV), relative to the non-replicating vector (rLCMV). We also performed mechanistic validation of our scRNA-Seq data. In particular, we evaluated the mechanistic roles of IFN-I by treating tumor-bearing mice with an IFN-I receptor–blocking antagonist (αIFNAR1 antibody, clone MAR1-5A3), which has been used in prior studies to block the IFN-I pathway (12, 19-22). Blockade of the IFN-I pathway significantly blunted the antitumoral efficacy of r3LCMV therapy (**Supplemental Figure 6**), suggesting that IFN-I could play a role in the antitumoral effect.

Next, we performed three series of experiments to determine the tumor-intrinsic versus host-intrinsic roles of IFN-I. In our first model, we challenged mice with B16 melanoma cells lacking IFNAR1 (B16 *Ifnar1*-/-) (**Figure 6B)**. These mice lacking IFN-I signaling specifically on tumor cells exhibited potent antitumoral responses and improved survival after r3LCMV treatment, suggesting that tumor-intrinsic IFN-I was dispensable (**Figure 6, C-D)**. In our second model, we challenged *Ifnar1-/-* mice with B16 melanoma cells. In this model, where the host cells could not sense IFN-I, we observed that the antitumoral effect

was modest and all mice succumbed within 4 weeks, suggesting that host-intrinsic IFN-I was important (**Figure 6, E-G**). In our third model, we challenged *Ifnar1*-/- mice with B16 *Ifnar1*-/- melanoma cells. In this third model, where both the host and the tumor are unable to sense IFN-I, the antitumoral effect of r3LCMV was dampened and there was no significant improvement in survival following r3LCMV therapy (**Figure 6, H-J**). These data suggest that host-intrinsic IFN-I signaling is critical for the antitumoral effect of r3LCMV therapy.

r3LCMV treatment induces antitumoral effects without the need for NK cells, macrophages, or MyD88.

Since the scRNA-Seq studies showed enrichment in NK cells and macrophages within the tumor upon r3LCMV treatment, we examined the contribution of these cells in tumor control. We first challenged mice with B16 melanoma tumors and then depleted NK cells continuously with an NK cell-depleting antibody to determine if the antitumoral effect of r3LCMV is mediated by NK cells. Our results indicate that NK cell depletion did not abrogate tumor control by the r3LCMV treatment (**Supplemental Figure 7, A-B**). Similarly, continuous depletion of macrophages using clodronate liposomes did not abrogate tumor control after r3LCMV treatment (**Supplemental Figure 7, C-D**). Altogether, the antitumoral effect of r3LCMV did not require NK cells and macrophages. In addition, we examined whether the antitumoral effects of r3LCMV were dependent on MyD88, which is an adaptor protein downstream of most Toll-like receptors (TLR) and that is considered to play a central role in innate immune responses. Interestingly, the

r3LCMV therapy was still effective in tumor-bearing *MyD88*-/- mice, demonstrating that MyD88 was not required for the antitumoral effect (**Figure 7**).

r3LCMV induces a long-lasting antitumoral state.

Tumors can recur throughout the lifespan of the host. In our experiments, all control PBS treated mice succumbed to the B16 melanoma challenge within weeks of tumor challenge, whereas a fraction of r3LCMV treated mice typically survived. We interrogated whether mice that had cleared tumors (following r3LCMV therapy) developed immune memory to the tumor. Surviving mice that were previously treated with r3LCMV and that had cleared B16 tumors showed enhanced tumor control following a secondary tumor challenge, relative to control naïve mice (**Supplemental Figure 8**), suggesting that r3LCMV induced a memory response to the tumor.

Until now, all of our r3LCMV treatments have been in tumor-bearing mice to examine its effect as a therapeutic regimen for cancer. But we also performed the "inverse" experiment by first treating mice with r3LCMV and then challenging them with B16 tumors several weeks after (**Figure 8A**). Treatment of non-tumor bearing mice with r3LCMV induced pro-inflammatory cytokines in serum, including IFN-I (**Figure 8B**). When challenged three weeks later with B16 melanoma, these r3LCMV-immune mice exhibited improved tumor control relative to r3LCMV-naïve mice (**Figure 8C**). Since LCMV does not share any epitopes with the B16 melanoma, this observation suggested induction of trained immunity. Trained immunity is a poorly understood process by which prior infections can trigger epigenetic changes in the innate immune system, resulting in

antigen-nonspecific immune protection against unrelated antigens (23). Prior studies have suggested a role for IFN-I in promoting trained immunity (24, 25), motivating us to examine its role. We first treated naïve mice with r3LCMV, and after three weeks, we treated these mice with control antibodies or IFNAR1 blocking antibodies, followed by B16 tumor challenge (**Figure 8D**). Interestingly, tumor control and survival in r3LCMV-immune mice were severely impaired when the IFN-I pathway was blocked, demonstrating a role for IFN-I (**Figure 8, E-F**). Overall, we demonstrate that r3LCMV vectors potentiate tumor control when they are administered after or before tumor challenges, suggesting not only therapeutic but also preventive antitumoral effects.

Discussion:

Tumor vaccines based on recombinant viruses expressing a tumor antigen payload or oncolytic viruses that lyse tumor cells have emerged as promising anticancer agents due to their ability to activate innate and adaptive immune responses, and directly kill cancer cells. For example, enteric cytopathic human orphan virus type 7 (ECHO-7) is currently being used for melanoma due to its ability to lyse tumor cells (26). In addition, an adenovirus-based vector is used for head and neck cancer; and an HSV-based vector is used for recurrent melanoma (2, 27). Less work has been done with nonlytic viruses that do not express any tumor antigen payload and do not directly kill tumor cells. Recently, LCMV vectors encoding HPV16 antigens started clinical trials for the treatment of HPV-related cancers. LCMV is a non-lytic arenavirus in clinical development as a vaccine vector to deliver tumor antigens to the immune system. LCMV does not directly lyse tumor cells, but it induces potent innate and adaptive immune responses that can eliminate infected cells. LCMV is also relatively proficient at evading antibody responses, allowing its re-utilization as a vaccine vector in a seropositive host (8, 28).

Prior research has shown that LCMV vectors can outperform protective efficacy elicited by other viral vector platforms, including Ad5 and poxvirus vectors (7, 29). When tumor-bearing mice are immunized with LCMV vectors containing the tumor antigen, they demonstrate stronger antitumor control relative to mice immunized with Ad5 or poxvirus vectors containing the same tumor antigen. However, ongoing clinical trials with LCMV vectors engineered to express tumor antigens have not assessed the potential

contribution of bystander (tumor non-specific) responses or whether immune activation by the viral vector itself can modulate tumor control.

Prior studies using models of therapeutic vaccination have shown that tumor-specific T cells play a critical antitumoral role in LCMV vector-based cancer therapy (7, 11), but it remains unclear whether LCMV vectors that do not express any tumor antigen can also exert antitumoral responses. Historically, the use of the viral vectors as cancer vaccines requires knowledge of the specific neoantigens or tumor-associated antigens encoded by the tumor, which may vary between different patients and tumor types. In our study, however, we utilized a “generic” r3LCMV platform that does not encode any tumor antigen. Since the r3LCMV vector and the tumor do not share any antigenic sequence, the antitumoral effect that we report could be considered bystander. Earlier studies by Lang and others have shown that infection of tumor-bearing mice with chronic virulent strains of LCMV can improve tumor control, suggesting also a bystander antitumoral effect (30-33). However, safety concerns of using live LCMV have deemed this approach hard to translate to humans. A prior clinical trial used live LCMV in cancer patients, but these patients died with evidence of multi-organ LCMV infection upon necropsy (34). These patients were in the late stages of lymphoma and it was unclear if for that reason they succumbed; one patient showed bacterial infection at the time of death so it was unclear if death was caused by the chronic LCMV infection or the bacterial infection. Chronic LCMV infection can also render the host more susceptible to other diseases due to the generalized immunosuppression associated with persistent viral infection (35). Considering these findings, attenuated replicating LCMV vectors represent a safer clinical

approach, given their high immunogenicity despite their limited ability to replicate. We report their safety and efficacy even in *Rag1*-/- mice.

In our study, we used an attenuated r3LCMV vector that replicates substantially lower than the parental virus but is still able to trigger a robust innate and adaptive immune response. Very low levels of systemic virus can be detected 72 hr after infection with attenuated r3LCMV, with mice showing only a very transient viremia near the limit of detection (<5 PFU/mL) with no weight loss or signs of disease (12). Our studies suggest that T cells, B cells, NK cells, and macrophages (as well as other phagocytes that can be depleted by clodronate liposomes like monocytes, dendritic cells, and neutrophils (36)) are not absolutely necessary for the antitumoral effect of r3LCMV. However, we found that activation of virus-specific CD8 T cells can facilitate tumor control by r3LCMV, as shown by our P14 adoptive transfer studies. We also demonstrated a critical role for host-intrinsic IFN-I signaling. Future studies will examine the contribution of IFN-I signaling on more specific immune subsets, such as dendritic cells and monocytes. In addition, we demonstrated that *MyD88*-/- mice respond to the r3LCMV therapy, which suggests that this major component of innate immunity is also dispensable for the antitumoral effect. It is possible that in the absence of MyD88, other adaptor molecules may compensate for the defects in innate immunity. Overall, the antitumoral effects of r3LCMV seem to engage multiple immune mechanisms, besides adaptive and innate (MyD88-dependent) immunity. Although unlikely, it is important to consider the potential for genetic recombination for r3LCMV vectors, and future studies should examine safety with these vectors more rigorously. Our data also suggest that r3LCMV induces trained immunity to

the tumor, since prior treatment with r3LCMV rendered the mice significantly more resistant to subsequent tumor challenges. In this context, IFN-I seemed to be mechanistically important. In summary, we demonstrate that attenuated r3LCMV vectors exert antitumoral effects in great part via IFN-I and that they are effective even in immunodeficient hosts without adaptive immunity. These studies are important for the development of LCMV-based therapies for cancer and for improving the mechanistic understanding of how nonlytic viral vectors modulate tumor immunity.

Limitations of the study

Absence of host-intrinsic IFN-I signaling limits the antitumor efficacy of r3LCMV, yet mice devoid of host-intrinsic IFN-I signaling show partial tumor control upon r3LCMV treatment, suggesting that other immune pathways may contribute to the antitumoral effects. Future studies will examine the contribution of other innate immune pathways that do not depend on MyD88 and examine more thoroughly how r3LCMV mediates trained immunity to tumors.

Materials and Methods:

Mice, tumor challenges, and LCMV vector treatments:

Sex as a biological variable: Our study examined male and female animals, and similar findings are reported for both sexes. Experiments were performed with 6-8-week-old wild-type mice (half males and half females) from Jackson laboratories, Bar Harbor, ME (C57BL/6, Stock No: 000664; BALB/c, Stock No: 000651; *Ifnar1*-/-, Stock No: 028288; *Rag1*-/-, Stock 002216; *MyD88*-/- mice, Stock No: 009088). Mice were challenged subcutaneously with 10^6 B16 melanoma cells, MC38 colon adenocarcinoma cells, and CT26 colon carcinoma cells and r3LCMV treatments started at day 5. Tumor volume was calculated as follows: Length x Width x Width x 1/2. Mouse challenges were performed at Northwestern University following BL2 guidelines with approval by the Institutional Animal Care and Use Committee (IACUC).

Cells and viruses:

We used a murine melanoma cell line: B16 (gift from Dr. Chyung-Ru Wang at Northwestern University, Chicago); B16-OVA melanoma cell line (gift from Dr. Jennifer Wu at Northwestern University, Chicago); B16-b2M -/- cells (gift from Dr. Omar Abdel-Wahab at Memorial Sloan Kettering Cancer Center, New York, NY), B16- *Ifnar1-/-* KO and B16-*Ifngr1-/-* cells (Invivogen), MC38 (ATCC), and CT26 (ATCC). The tumor cells were cultured in DMEM (GIBCO, Cat# 11965-092) with 10% Fetal Bovine Serum (Sigma-Aldrich, Cat# F0926), 1% L- Glutamine (GIBCO, Cat# 25030-081), and 1% Penicillin and Streptomycin (GIBCO, Cat#15140-122) in 37°C 5% CO_2 incubator. BHK-21 cells (ATCC,

Cat# CCL-10) were used for production of LCMV, VSV, and YFV-17D. Vero E6 cells (ATCC, Cat# CRL-1586) were used for titration of r3LCMV, VSV, and YFV-17D. BHK-21 and Vero E6 cells were cultured in EMEM (ATCC, Cat# 30-2003) with 10% FBS, 1% L-Glutamine, and 1% Penn/Strep in 37 °C 5% CO_2 incubator. Non-replicating (rLCMV) vectors expressing GFP (used in Figures 2, 6A and Supplemental Figure 1) were a kind gift from Hookipa Pharma Inc (Viena, Austria). For the rest of the experiments, we used replicating (r3LCMV) vectors expressing GFP, which were made using DNA plasmids from Dr. Juan Carlos De La Torre (Scripps Research Institute, La Jolla, CA). The LCMV strain lacking the GP33-41 epitope (GP35V→A escape mutation, which cannot be recognized by P14 cells) was derived from a prior study (17). This LCMV variant was used to examine the role of virus-specific CD8 T cell activation in tumor control.

Adoptive cell transfer:

CD8 T cells were purified from spleens of transgenic P14 mice, using a negative selection isolation kit (STEMCELL Technologies), and purity was confirmed to be >97%. $5x10^6$ CD8 T cells were injected into a mouse intravenously, one day before viral infection.

Antibody treatments, cell depletions:

All Antibodies for in vivo treatments were purchased from BioXCell (Lebanon, NH) or Leinco (Fenton, MO), and were diluted in sterile PBS and injected intraperitoneally (i.p.). PD-L1 blocking antibodies (clone 10F.9G2) were administered at 200 μg, every three days, five times, as previously shown (37). B7.1 and B7.2 blocking antibodies (clones 16-10A1 and GL-1, respectively) were administered at 200 μg each, every three days.

IFNAR1 blocking antibodies (clone MAR1-5A3) were administered at 200 μg, every three days, five times. This MAR1-5A3 antibody binds to interferon α/β receptor subunit 1 (clone IFNAR1) and blocks binding to interferons α/β, abrogating the induction of ISGs in vivo (20, 22, 38-40). NK cell depleting antibodies (clone NK1.1 PK136) were administered at 500 μg, every 2 days, five times. CD4 T cell depleting antibodies (clone GK1.5) were administered at 200 μg, two times, and CD8 T cell depleting antibodies (clone 2.43) were administered at 200 μg, every three days, five times (starting on the day of r3LCMV treatment). Diphtheria toxin (Sigma-Aldrich) was administered at 1 μg i.p. (diluted in PBS), on days 0, 1, 4, 7, and 10 of r3LCMV therapy. This dose was similar to prior studies, using Foxp3-DTR knock-in mice on a C57BL/6 background (14, 41). Clodronate liposomes (SKU# CLD-8909, Encapsula NanoSciences, Brentwood, TN) were administered at 200 μg every 3 days, four times.

Quantification of viral titers:

Viral titers were quantified as described previously (42). In brief, $5x10^5$ of Vero E6 cells were plated onto each well in 6-well plates, and after 24~48 hours when they reached ~95% confluency, the media were removed and 200 μL of serial dilutions (of viral stock or tissue homogenates) were added dropwise on top of the monolayer of the cells. Plates were rocked every 10 min in a 37 °C, 5% CO_2 incubator for 1 hour. 200 μL of media was aspirated out, and the monolayers were gently overlaid with a 1:1 mixture of 2x 199 media (20% FBS, 2% Pen/Strep, 2% L-glutamine) and 1% agarose at 37°C. After 4 days, a second overlay was added, consisting of a 1:1 solution of 2x 199 media, 1% agarose,

and 1:50 of neutral red. Overlay was removed on day 5 and plaques were counted using a conventional light microscope.

Flow cytometry:

MHC class I monomers (K^bSIINFEKL or D^bGP33,) were used for detecting virus-specific CD8 T cells, and were obtained from the NIH tetramer facility located at Emory University. MHC I monomers were tetramerized in-house. Single cell suspensions were stained with live/dead fixable dead cell stain (APC- Cy7, Invitrogen, cat# L34976A), anti-mouse CD8α (clone: 53–6.7, PerCP-Cy5.5, BD Pharmingen, cat # 551162; clone: 53–6.7, FITC, BD Pharmingen, cat# 553031; clone: 53–6.7, APC, eBioscience, cat# 17-0081-83), anti-mouse CD4, (clone: RM4-5, PE-Cy7, eBioscience, cat# 25-0042-82; clone: RM4-5, Pacific Blue, eBioscience, cat# 57-0042- 82), anti-mouse CD44 (clone: IM7, FITC, BD Pharmingen, cat# 553133; clone: IM7, Pacific Blue, Biolegend, cat# 103020), anti-mouse CD80 (clone: 16-10A1, FITC, BD Pharmingen, cat# 553768), anti-mouse CD86 (clone: GL1, PE, BD Pharmingen, cat# 561963), anti- IFNAR1 (clone: MAR1-5A3, PE, Biolegend, cat# 127312), anti-mouse CD11b (clone: M1/70, Alexa Fluor 700, Biolegend, cat# 101222), anti-mouse CD11c (clone: N418, PerCP Cy5.5, Biolegend, cat# 117328; clone: N418, PE-Cy7, Biolegend, cat# 117318), anti-mouse CD90.1 (Thy1.1) (clone: HIS51, eFluor 450, eBioscience, cat# 48-0900-82; clone: HIS51, PE- Cy7, eBioscience, cat# 25-0900-82), anti-mouse CD90.2 (Thy1.2) (clone: 53-2.1, APC, eBioscience, cat# 17-0902-82), anti-mouse CD45.1 (clone: A20, PE-Cy7, Biolegend, cat# 110730; clone: A20, FITC, BD Pharmingen, cat# 553775), anti-mouse CD45.2 (clone: 104, PE, Biolegend, cat# 109808; clone: 104, FITC, BD Pharmingen, cat# 553772), anti-mouse TCR Va2 (clone:

B20.1, PE, BD Pharmingen, cat# 553289), anti- mouse CD279 (PD-1) (clone: RMP1-30, PE, Biolegend, cat# 109104; clone: RMP1-30, PE-Cy7, Biolegend, cat# 109110; clone: RMP1-30, FITC, eBioscience, cat# 11-9981- 85), anti-mouse CD274 (B7-H1, PD-L1) (clone: 10F.9G2, PE, Biolegend, cat# 124308), anti-mouse Foxp3 (clone: FJK-16s, APC, eBioscience, cat# 17-5773-82), anti-mouse CD25 (clone: 3C7, PerCP-Cy5.5, Biolegend, cat# 101911), anti-mouse B220 (clone: RA3-6B2, PerCP-Cy5.5, Biolegend, cat# 103236), and anti-mouse CD3 (clone: 17A2, Pacific blue, Biolegend, cat# 100214; clone: 17A2, Biotin, Biolegend, cat# 100244), anti- mouse Ly-6G (clone: RB6-8c5, Biotin, eBioscience, cat# 13-5931-85), anti-mouse NK1.1 (clone: PK136, Biotin, eBioscience, cat# 13-5941-85; clone: PK136, PE, BD Pharmingen, cat# 553165), anti-mouse CD19 (clone: eBio1D3, Biotin, eBioscience, cat# 13-0193-82), SA-BV421 (Biolegend, cat# 405225), SA-APC (Invitrogen, cat# S868), and SA-PE (Biolegend, cat# 405204). Flow cytometry samples were acquired with a Becton Dickinson Canto II or an LSRII and analyzed using FlowJo v10 (Treestar).

Tumor sectioning and immunofluorescence:

Tumors were fixed in PLP fixative solution for 24 hours at 4°C. The tumor samples were washed with PBS and cryoprotected for 24 hours at 4°C in a sucrose/PBS dilution. The fixed tissue samples were frozen in OCT on dry ice. Once the samples were frozen, they were kept in -80°C freezer until sectioning. The tissue samples were sectioned using a cryomicrotome with 10 µm thickness. The frozen sections were washed with PBS 2 times for 5 minutes each time and rinsed in 0.05% PBS-T. The slides were incubated with the blocking solution (PBS + 1% BSA + 5% goat serum) for 10 minutes. The slides were

stained with the primary and the secondary antibodies in the blocking solution for 2 hours and 1 hour, respectively. VL4 antibody (BioXCell) was used to detect LCMV antigen. After the primary and the secondary antibody staining, the slides were washed 2 times with PBS-T. The slides were washed with water and mounted with Vector AntiFade mounting medium. Slides were imaged at the Center for Advanced Microscopy (CAM) Cell Imaging Facility and Nikon Imaging Center at Northwestern University.

Multiplex cytokine/chemokine assay:

The mouse peripheral blood samples were collected in 1.5ml tubes 24 hours post-infection of LCMV. The blood samples were centrifugated at 15000 rpm in 4°C to separate the serum samples. The serum samples were collected and frozen in -80°C until its use. Multiplex cytokines/chemokines kit was purchased from Mesoscale Diagnostics LLC.

LCMV-specific ELISA:

Binding antibody titers were quantified using ELISA as described previously (12, 42-47), using LCMV GP as coating antigen. Briefly, 96-well, flat-bottom MaxiSorp plates (Thermo Fisher Scientific) were coated with 1 µg/mL of GP for 48 hours at 4°C. Plates were washed 3 times with wash buffer (PBS plus 0.05% Tween 20). Blocking was performed with blocking solution (200 µl PBS plus 0.05% Tween 20 plus 2% BSA) for 4 hr at room temperature. 6 µl of plasma samples were added to 144 µl of blocking solution in the first column of the plate, 3-fold serial dilutions were prepared for each sample, and plates were incubated for 1 hr at room temperature. Plates were washed 3 times with wash buffer. Goat anti-mouse IgG antibody tagged with streptavidin-HRP (Southern Biotech, 7105-05)

was diluted 1:400 in blocking buffer and incubated for 1 hr at room temperature. After washing plates 3 times with wash buffer, 100 µl/well SureBlue Substrate (SeraCare) was added for 1 min. The reaction was stopped using 100 µl/well KPL TMB Stop Solution (SeraCare). Absorbance was measured at 450 nm using a Spectramax Plus 384 (Molecular Devices).

Single-cell RNA sequencing (scRNA-seq):

5 different mice treated with r3LCMV and 5 different mice treated with vehicle (PBS) were enriched for CD45+ cells and pooled for single-cell sequencing, separately. Single-cell libraries were generated using 10x Genomics 3' kits. Cell Ranger (version 6.1.2) was used to demultiplex raw base call files (BCL) to FASTQ files and align reads to the Mouse genome (Ensembl version GRCm39 version 110) supplemented with LCMV genome (GenBank accession NC_004291.1 and NC_004294.1). For counting, Cell Ranger was run with the option to include reads spanning intron regions of genes during counting; all remaining default options were used. Count matrices were further analyzed in R (version 4.6.2), Bioconductor (version 3.17) and the R package Seurat (version 4.3.0.1). The R package SingleR (version 2.2.0) with the ImmGen reference was used to annotate the subset of each cell. Differential expression was performed by fitting a negative binomial generalized linear model to gene expression and a likelihood-ratio test for statical testing. Benjamini-Hoshberg adjustment was used to correct for multiple testing and cutoff of 5% false-positive was considered significant. scRNA-seq was performed at the Northwestern University NUSeq core.

Statistical analysis:

Statistical analyses are indicated on the figure legends. Statistical significance was established at $p \leq 0.05$. In the figures showing tumor control over time, the p-values were calculated based on the tumor sizes at the last time point shown. Data were analyzed using Prism (Graphpad).

Study approval:

Mouse studies were performed at Northwestern University following BSL-2 guidelines with approval of the Institutional Animal Care and Use Committee (IACUC), under protocol #IS00003324.

Data availability:

scRNA-seq data are uploaded in GEO under the accession number GSE255499 (https://www.ncbi.nlm.nih.gov/geo/query/acc.cgi). Other data can be requested from the corresponding author. Supporting data values associated with the main manuscript and supplemental material is included in the Supporting Data Values files.

Author Contributions:

Y.R.C and B.A. performed most of the mouse tumor challenge and immunogenicity experiments. Authorship order was decided mutually by these two co-first authors. T.D. and N.I. helped to perform some of the mouse experiments. S. F. analyzed the gene expression data. P.P.M. designed the experiments and secured funding. P.P.M. wrote the paper with feedback from all authors. The gene expression analysis in this research

was supported in part through the computational resources and staff contributions provided by the Genomics Compute Cluster, which is jointly supported by the Feinberg School of Medicine, the Center for Genetic Medicine, the Feinberg's Department of Biochemistry and Molecular Genetics, the Office of the Provost, the Office for Research, and the Northwestern Information Technology.

Acknowledgements:

We thank Dr. Juan Carlos De La Torre (Scripps Research Institute, La Jolla, CA), Dr. Stephen Waggoner and Dr. Carolyn Rydyznski (Cincinnati Children's Medical Center, Cincinnati, OH) for technical assistance making the r3LCMV vectors. We thank Drs. Jennifer Wu, Bin Zhang, and Chyung-Ru Wang for discussions. We also thank Hookipa Biotech for sharing rLCMV vectors and for helpful discussions. We thank Dr. Rebecca Obeng for guidance on the tissue sectioning and immunostaining of tumor samples. We thank Dr. Ching Man Wai at the NUSeq core for help with the scRNA-Seq experiments. Several images were created with Biorender.com. This work was possible with a grant from the National Institute on Drug Abuse (NIDA, DP2DA051912) to P.P.M., an Institutional Research Grant (IRG-15-173-21) from the American Cancer Society to P.P.M., a pilot grant from the Lurie Cancer Center at Northwestern University.

1. Bommareddy PK, Shettigar M, and Kaufman HL. Integrating oncolytic viruses in combination cancer immunotherapy. *Nat Rev Immunol.* 2018;18(8):498-513.
2. Andtbacka RH, Kaufman HL, Collichio F, Amatruda T, Senzer N, Chesney J, et al. Talimogene Laherparepvec Improves Durable Response Rate in Patients With Advanced Melanoma. *J Clin Oncol.* 2015;33(25):2780-8.
3. Popkin DL, Teijaro JR, Lee AM, Lewicki H, Emonet S, de la Torre JC, et al. Expanded potential for recombinant trisegmented lymphocytic choriomeningitis viruses: protein production, antibody production, and in vivo assessment of biological function of genes of interest. *J Virol.* 2011;85(15):7928-32.
4. Emonet SF, Garidou L, McGavern DB, and de la Torre JC. Generation of recombinant lymphocytic choriomeningitis viruses with trisegmented genomes stably expressing two additional genes of interest. *Proc Natl Acad Sci U S A.* 2009;106(9):3473-8.
5. Bonilla WV, Kirchhammer N, Marx AF, Kallert SM, Krzyzaniak MA, Lu M, et al. Heterologous arenavirus vector prime-boost overrules self-tolerance for efficient tumor-specific CD8 T cell attack. *Cell Rep Med.* 2021;2(3):100209.
6. Schmidt S, Bonilla WV, Reiter A, Stemeseder F, Kleissner T, Oeler D, et al. Live-attenuated lymphocytic choriomeningitis virus-based vaccines for active immunotherapy of HPV16-positive cancer. *Oncoimmunology.* 2020;9(1):1809960.
7. Kallert SM, Darbre S, Bonilla WV, Kreutzfeldt M, Page N, Muller P, et al. Replicating viral vector platform exploits alarmin signals for potent CD8(+) T cell-mediated tumour immunotherapy. *Nat Commun.* 2017;8:15327.
8. Penaloza MacMaster P, Shields JL, Alayo QA, Cabral C, Jimenez J, Mondesir J, et al. Development of novel replication-defective lymphocytic choriomeningitis virus vectors expressing SIV antigens. *Vaccine.* 2017;35(1):1-9.
9. Belnoue E, Vogelzang A, Nieuwenhuizen NE, Krzyzaniak MA, Darbre S, Kreutzfeldt M, et al. Replication-Deficient Lymphocytic Choriomeningitis Virus-Vectored Vaccine Candidate for the Induction of T Cell Immunity against Mycobacterium tuberculosis. *Int J Mol Sci.* 2022;23(5).
10. Lauterbach H, Schmidt S, Katchar K, Qing X, Iacobucci C, Hwang A, et al. Development and Characterization of a Novel Non-Lytic Cancer Immunotherapy Using a Recombinant Arenavirus Vector Platform. *Front Oncol.* 2021;11:732166.
11. Ring SS, Cupovic J, Onder L, Lutge M, Perez-Shibayama C, Gil-Cruz C, et al. Viral vector-mediated reprogramming of the fibroblastic tumor stroma sustains curative melanoma treatment. *Nat Commun.* 2021;12(1):4734.
12. Palacio N, Dangi T, Chung YR, Wang Y, Loredo-Varela JL, Zhang Z, et al. Early type I IFN blockade improves the efficacy of viral vaccines. *J Exp Med.* 2020;217(12).
13. Bos PD, Plitas G, Rudra D, Lee SY, and Rudensky AY. Transient regulatory T cell ablation deters oncogene-driven breast cancer and enhances radiotherapy. *J Exp Med.* 2013;210(11):2435-66.
14. Penaloza-MacMaster P, Kamphorst AO, Wieland A, Araki K, Iyer SS, West EE, et al. Interplay between regulatory T cells and PD-1 in modulating T cell exhaustion and viral control during chronic LCMV infection. *J Exp Med.* 2014;211(9):1905-18.

15. Lu SX, De Neef E, Thomas JD, Sabio E, Rousseau B, Gigoux M, et al. Pharmacologic modulation of RNA splicing enhances anti-tumor immunity. *Cell.* 2021;184(15):4032-47 e31.
16. Goldrath AW, and Bevan MJ. Low-affinity ligands for the TCR drive proliferation of mature CD8+ T cells in lymphopenic hosts. *Immunity.* 1999;11(2):183-90.
17. Blattman JN, Wherry EJ, Ha SJ, van der Most RG, and Ahmed R. Impact of epitope escape on PD-1 expression and CD8 T-cell exhaustion during chronic infection. *J Virol.* 2009;83(9):4386-94.
18. Shankaran V, Ikeda H, Bruce AT, White JM, Swanson PE, Old LJ, et al. IFNgamma and lymphocytes prevent primary tumour development and shape tumour immunogenicity. *Nature.* 2001;410(6832):1107-11.
19. Bhattacharyya M, Madden P, Henning N, Gregory S, Aid M, Martinot AJ, et al. Regulation of CD4 T cells and their effects on immunopathological inflammation following viral infection. *Immunology.* 2017;152(2):328-43.
20. Wilson EB, Yamada DH, Elsaesser H, Herskovitz J, Deng J, Cheng G, et al. Blockade of chronic type I interferon signaling to control persistent LCMV infection. *Science.* 2013;340(6129):202-7.
21. Wang Y, Chung YR, Eitzinger S, Palacio N, Gregory S, Bhattacharyya M, et al. TLR4 signaling improves PD-1 blockade therapy during chronic viral infection. *PLoS Pathog.* 2019;15(2):e1007583.
22. Teijaro JR, Ng C, Lee AM, Sullivan BM, Sheehan KC, Welch M, et al. Persistent LCMV infection is controlled by blockade of type I interferon signaling. *Science.* 2013;340(6129):207-11.
23. Netea MG, Quintin J, and van der Meer JW. Trained immunity: a memory for innate host defense. *Cell Host Microbe.* 2011;9(5):355-61.
24. Ochando J, Mulder WJM, Madsen JC, Netea MG, and Duivenvoorden R. Trained immunity - basic concepts and contributions to immunopathology. *Nat Rev Nephrol.* 2023;19(1):23-37.
25. Li W, Moorlag S, Koeken V, Roring RJ, de Bree LCJ, Mourits VP, et al. A single-cell view on host immune transcriptional response to in vivo BCG-induced trained immunity. *Cell Rep.* 2023;42(5):112487.
26. Donina S, Strele I, Proboka G, Auzins J, Alberts P, Jonsson B, et al. Adapted ECHO-7 virus Rigvir immunotherapy (oncolytic virotherapy) prolongs survival in melanoma patients after surgical excision of the tumour in a retrospective study. *Melanoma Res.* 2015;25(5):421-6.
27. Liang M. Oncorine, the World First Oncolytic Virus Medicine and its Update in China. *Curr Cancer Drug Targets.* 2018;18(2):171-6.
28. Pinschewer DD, Perez M, Jeetendra E, Bachi T, Horvath E, Hengartner H, et al. Kinetics of protective antibodies are determined by the viral surface antigen. *J Clin Invest.* 2004;114(7):988-93.
29. Flatz L, Hegazy AN, Bergthaler A, Verschoor A, Claus C, Fernandez M, et al. Development of replication-defective lymphocytic choriomeningitis virus vectors for the induction of potent CD8+ T cell immunity. *Nat Med.* 2010;16(3):339-45.

30. Haas VH, and Nadel EM. Effect of the virus of lymphocytic choriomeningitis on the course of leukemia in guinea pigs and mice. *J Natl Cancer Inst.* 1956;17(2):221-31.
31. Eiselein J, and Biggs MW. Observations with a variant of lymphocytic choriomeningitis virus in mouse tumors. *Cancer Res.* 1970;30(7):1953-7.
32. Molomut N, and Padnos M. Inhibition of transplantable and spontaneous murine tumours by the M-P virus. *Nature.* 1965;208(5014):948-50.
33. Kalkavan H, Sharma P, Kasper S, Helfrich I, Pandyra AA, Gassa A, et al. Spatiotemporally restricted arenavirus replication induces immune surveillance and type I interferon-dependent tumour regression. *Nat Commun.* 2017;8:14447.
34. Horton J, Hotchin JE, Olson KB, and Davies JN. The effects of MP virus infection in lymphoma. *Cancer Res.* 1971;31(8):1066-8.
35. Kohler M, Ruttner B, Cooper S, Hengartner H, and Zinkernagel RM. Enhanced tumor susceptibility of immunocompetent mice infected with lymphocytic choriomeningitis virus. *Cancer Immunol Immunother.* 1990;32(2):117-24.
36. Culemann S, Knab K, Euler M, Wegner A, Garibagaoglu H, Ackermann J, et al. Stunning of neutrophils accounts for the anti-inflammatory effects of clodronate liposomes. *J Exp Med.* 2023;220(6).
37. Barber DL, Wherry EJ, Masopust D, Zhu B, Allison JP, Sharpe AH, et al. Restoring function in exhausted CD8 T cells during chronic viral infection. *Nature.* 2006;439(7077):682-7.
38. Bhattacharyya M, Madden P, Henning N, Gregory S, Aid M, Martinot A, et al. Regulation of CD4 T cells and their effects on immunopathological inflammation following viral infection. *Immunology.* 2017.
39. Sheehan KC, Lai KS, Dunn GP, Bruce AT, Diamond MS, Heutel JD, et al. Blocking monoclonal antibodies specific for mouse IFN-alpha/beta receptor subunit 1 (IFNAR-1) from mice immunized by in vivo hydrodynamic transfection. *J Interferon Cytokine Res.* 2006;26(11):804-19.
40. Pinto AK, Daffis S, Brien JD, Gainey MD, Yokoyama WM, Sheehan KC, et al. A temporal role of type I interferon signaling in CD8+ T cell maturation during acute West Nile virus infection. *PLoS Pathog.* 2011;7(12):e1002407.
41. Kim JM, Rasmussen JP, and Rudensky AY. Regulatory T cells prevent catastrophic autoimmunity throughout the lifespan of mice. *Nat Immunol.* 2007;8(2):191-7.
42. Dangi T, Chung YR, Palacio N, and Penaloza-MacMaster P. Interrogating Adaptive Immunity Using LCMV. *Curr Protoc Immunol.* 2020;130(1):e99.
43. Sanchez S, Palacio N, Dangi T, Ciucci T, and Penaloza-MacMaster P. Fractionating a COVID-19 Ad5-vectored vaccine improves virus-specific immunity. *Sci Immunol.* 2021;6(66):eabi8635.
44. Dangi T, Sanchez S, Lew MH, Awakoaiye B, Visvabharathy L, Richner JM, et al. Pre-existing immunity modulates responses to mRNA boosters. *Cell Rep.* 2023;42(3):112167.
45. Dangi T, Sanchez S, Class J, Richner MC, Visvabharathy L, Chung YR, et al. Improved control of SARS-CoV-2 by treatment with nucleocapsid-specific monoclonal antibody. *J Clin Invest.* 2022.
46. Dangi T, Palacio N, Sanchez S, Park M, Class J, Visvabharathy L, et al. Cross-protective immunity following coronavirus vaccination and coronavirus infection. *J Clin Invest.* 2021;131(24).

47. Dangi T, Class J, Palacio N, Richner JM, and Penaloza MacMaster P. Combining spike- and nucleocapsid-based vaccines improves distal control of SARS-CoV-2. *Cell Rep.* 2021;36(10):109664.

Figure 1

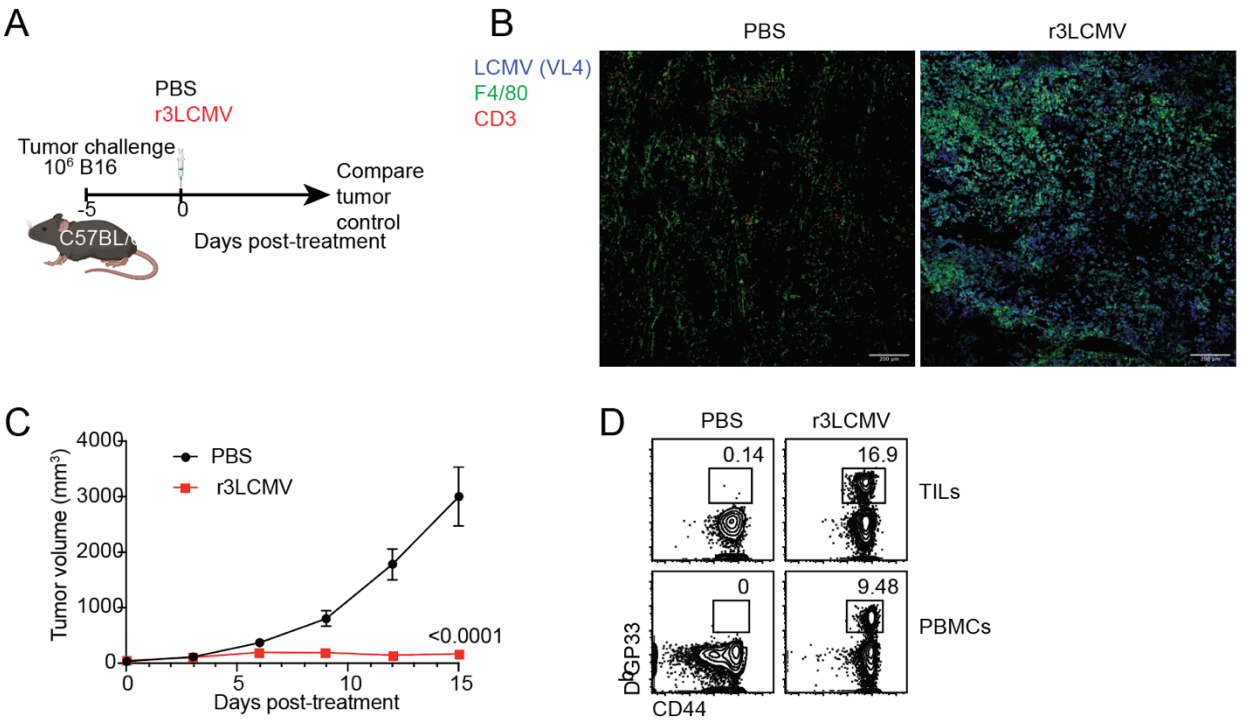

Figure 1. r3LCMV replicates in B16 tumors and improves tumor control. (**A**) Experiment outline for evaluating whether r3LCMV improves tumor control. (**B**) Representative immunofluorescence staining in tumor sections at day 4 post-treatment. We used an LCMV nucleoprotein-specific antibody (clone VL4) to label virus-infected cells in tumor sections. Scale bars represent 200 μm. (**C**) Tumor control. (**D**) Representative FACS plots showing LCMV-specific CD8 T cell responses at day 7 post-treatment (gated on live CD8 T cells). Mice were treated intratumorally with $2x10^5$ focus forming units (FFU) of r3LCMV, five days after subcutaneous tumor challenge. Before r3LCMV treatments, groups were distributed evenly according to tumor size. Data are pooled from 2 experiments (one experiment with n=5 per group and another with n=7 per group). Error bar represents SEM. Indicated P values were calculated by the Mann–Whitney test.

Figure 2

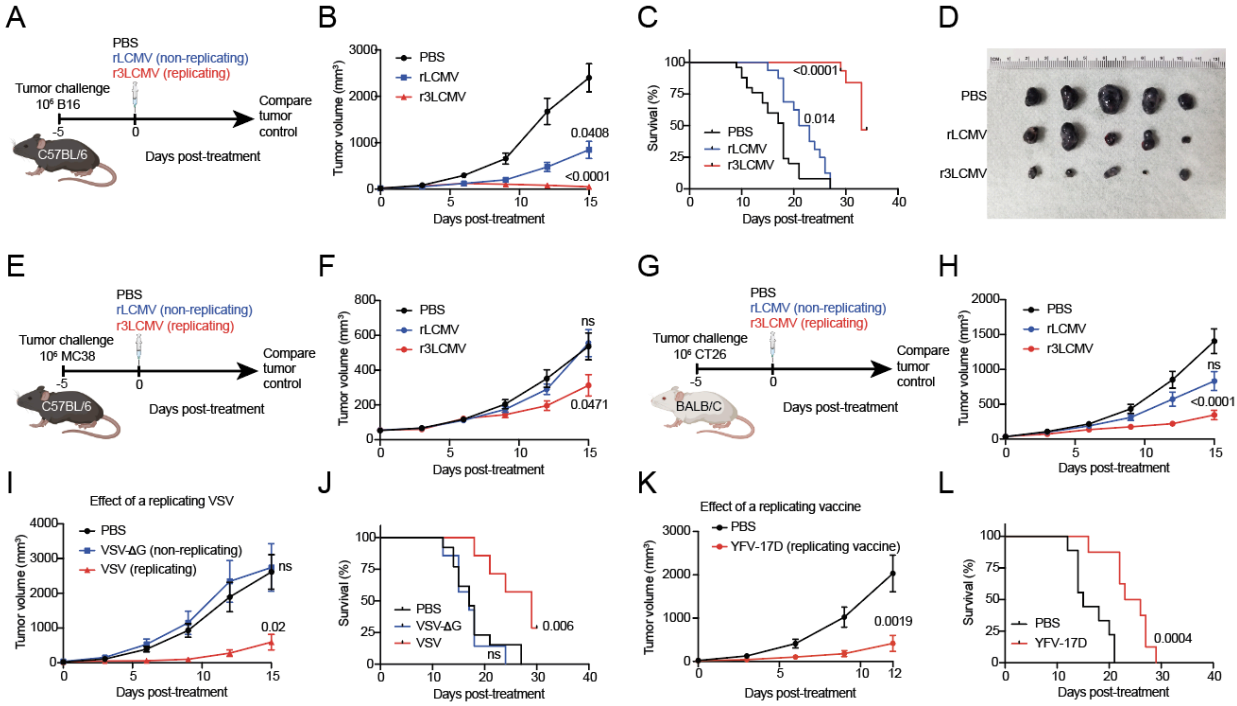

Figure 2. Comparing the antitumoral effects by replicating versus non-replicating viral vectors. (**A-D**) Effect of replicating (r3LCMV) versus non-replicating (rLCMV) vectors in the B16 melanoma model in C57BL/6 mice. (**A**) Experiment outline. The set up was similar to Figure 1 but comparing replicating versus non-replicating LCMV vectors. (**B**) Tumor control. (**C**) Survival. (**D**) Representative images of tumors at day 8 post-treatment. (**E-F**) Effect of replicating versus non-replicating LCMV vectors in the colon adenocarcinoma model in C57BL/6 mice. (**E**) Experiment outline. (**F**) Tumor control. (**G-H**) Effect of replicating versus non-replicating LCMV vectors in the CT26 colon carcinoma model in BALB/c mice. (**G**) Experiment outline. (**H**) Tumor control. (**I-J**) Effect of replicating versus non-replicating VSV in the B16 melanoma model in C57BL/6 mice. (**I**) Tumor control. (**J**) Survival. (**K-L**) Effect of replicating YFV-17D vaccine in the B16 melanoma model in C57BL/6 mice. (**K**) Tumor control. (**L**) Survival. Mice were treated intratumorally

with $2x10^5$ FFU of the indicated viruses, five days after tumor challenge. LCMV data are pooled from 2 experiments per tumor model (n=5-13 per group). VSV data are pooled from 2 experiments per tumor model (n=3-7 per group). YFV-17D data are pooled from 2 experiments per tumor model (n=4-5 per group). Error bar represents SEM. Indicated P values in the tumor volume plots were calculated by the Mann–Whitney test, or Kruskal-Wallis (Dunn's multiple comparison) test when comparing more than 2 groups. Indicated P values in the survival plots were calculated by the log rank test.

Figure 3

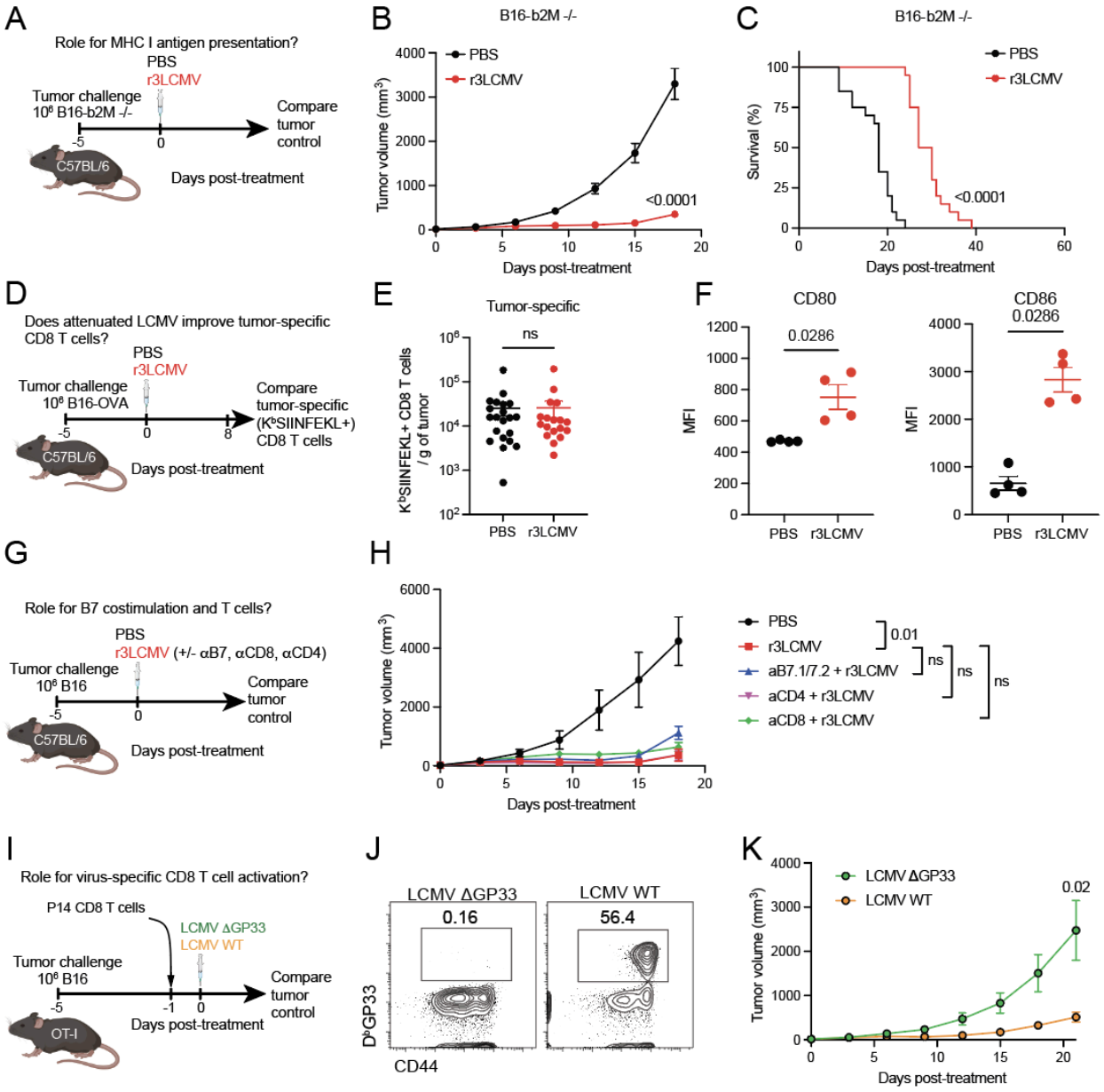

Figure 3. r3LCMV exerts antitumoral effects independent of CD8 T cells and B7/CD28 costimulation. (**A-C**) Effect of r3LCMV vectors in the B16 B2m -/- melanoma model. (**A**) Experiment outline for evaluating the role of MHC I. (**B**) Tumor control. (**C**) Survival. (**D-E**) Effect of LCMV vectors on tumor-specific CD8 T cell responses. (**D**) Experiment outline for measuring tumor-specific CD8 T cells in the tumor. (**E**) Tumor-specific CD8 T cells at day 8 post-treatment. (**F-G**) Upregulation of B7 costimulatory

molecules by r3LCMV. (**F**) CD80 and CD86 costimulatory molecules on DCs from tumor-draining lymph nodes. DCs were gated on live, CD3-, NK1.1-, Ly6G-, CD19-, CD11b+, CD11c+ at day 4 post-treatment. (**G-H**) Effect of B7 costimulation blockade, CD8 T cell depletion, and CD4 T cell depletion. B7.1/B7.2 blocking antibodies, CD8 T cell depleting antibodies, or CD4 T cell depleting antibodies were administered intraperitoneally every 3 days (see Materials and Methods for dosing information). (**G**) Experiment outline for evaluating the role of T cells and costimulation. (**H**) Tumor control. (**I-K**) Effect of virus-specific CD8 T cells. (**I**) Experiment outline for evaluating the role of virus-specific T cell activation. (**J**) Representative FACS plots showing P14 cell expansion in PBMCs at day 7 post-treatment. (**K**) Tumor control. Data from panels A-C are pooled from 2 experiments (one experiment with n=10 per group and another with n=10 per group). Data from panels D-E are pooled from 2 experiments (one experiment with n=9 per group and another with n=9-12 per group). Data from panel F are from 1 representative experiment (n=4 per group). Data from panels G-H are from 1 representative experiment (n=6-7 per group). Data from panels I-K are from 1 representative experiment (n=6-7 per group). Error bar represents SEM. Indicated P values in the tumor volume plots were calculated by the Mann–Whitney test, or Kruskal-Wallis (Dunn's multiple comparison) test when comparing more than 2 groups. Indicated P values in the survival plot were calculated by the log rank test.

Figure 4

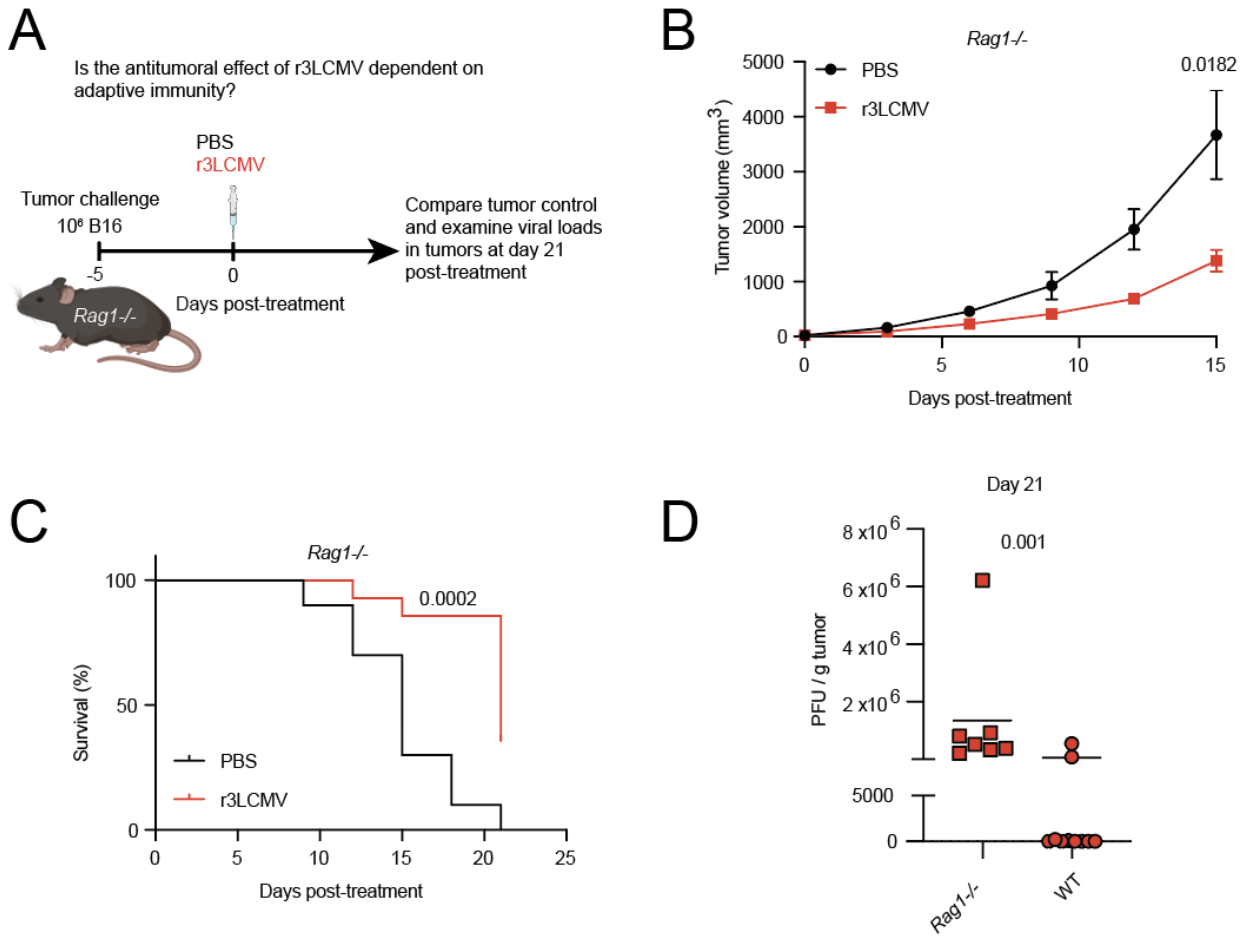

Figure 4. r3LCMV therapy improves tumor control in *Rag1*-/- mice. (**A**) Experiment outline. (**B**) Tumor control. (**C**) Survival. (**D**) Viral loads in tumors at day 21 post-treatment. Viral loads were quantified by plaque assays on Vero cell monolayers. Data from panels B-C are pooled from 2 experiments (one experiment with n=5 per group and another with n=5-9 per group). Data from panel D are from the tumors of 7 *Rag1*-/- mice that were r3LCMV treated and survived until day 21 (tumors of 10 wild-type mice that were r3LCMV treated and survived until day 21 are included for comparison). Error bar represents SEM. Indicated P values were calculated by the Mann–Whitney test, or log rank test when comparing survival.

Figure 5

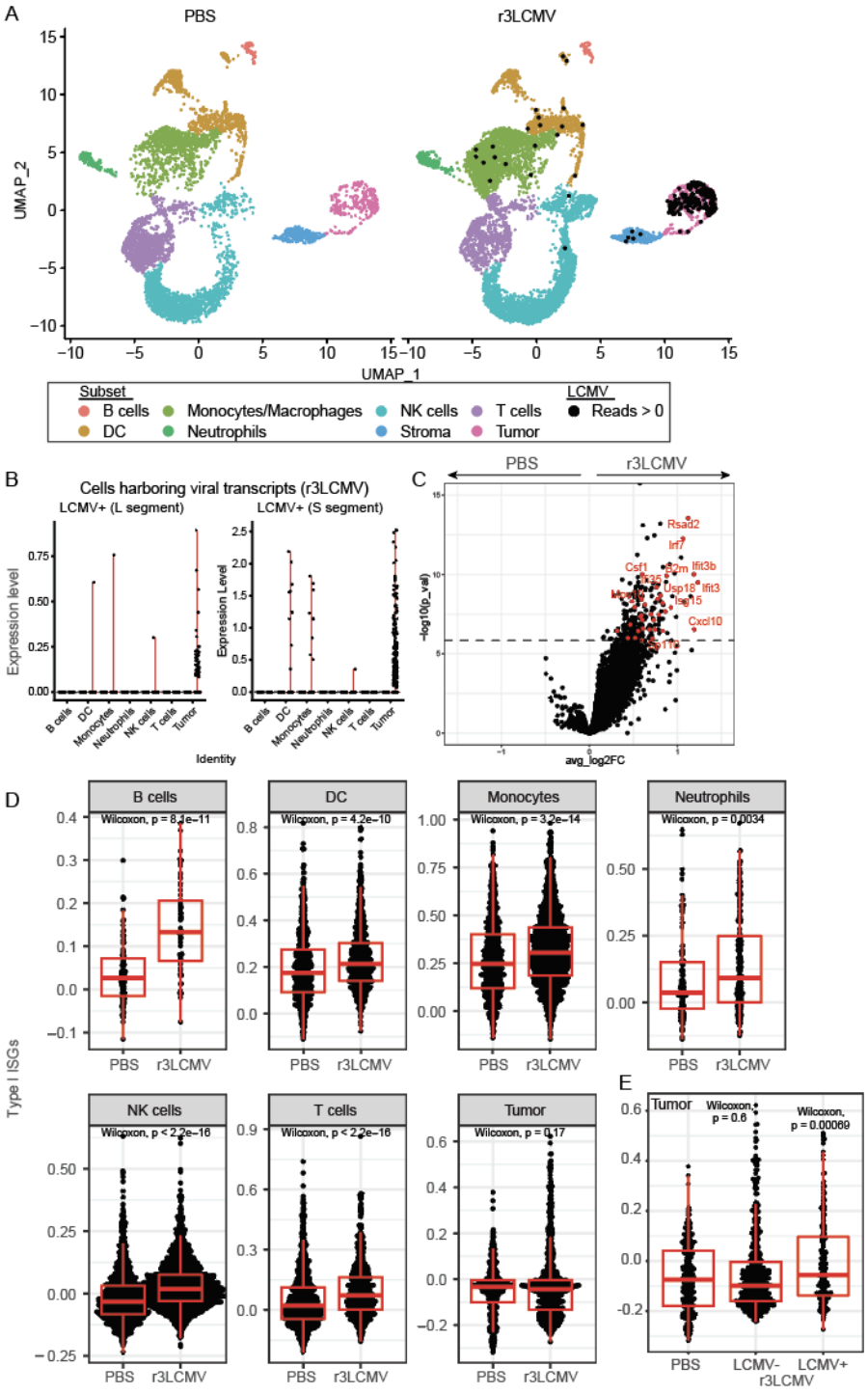

Figure 5. scRNA-Seq reveals enrichment of IFN-I responses by r3LCMV therapy. We performed gene expression analyses to understand the effects of r3LCMV on different cell subsets within the tumor microenvironment at day 4 post-treatment. (**A**) UMAP plots showing cell distribution based on RNA expression. Each cell is colored by its inferred subset (based on ImmGen database). Cells harboring LCMV reads are indicated by a black dot. (**B**) Level of expression of LCMV L and S transcripts on different cell subsets from r3LCMV treated mice. (**C**) Volcano plot showing the differential

expression of genes in tumor cells harboring LCMV reads versus those without LCMV reads. The dash line indicates p-value adjusted for multiple testing of 0.05. ISG are indicated in red. (**D**) Enrichment for ISG in different cell subsets. (**E**) ISG on tumor cells harboring LCMV or not harboring LCMV. This panel shows that tumor cells with LCMV reads express higher levels of ISG relative to tumor cells without LCMV reads. For each boxplot, the vertical line indicates the median, the box indicates the interquartile range, and the whiskers indicate 1.5 times the interquartile range. ~80% of cells were CD45+ (after MACS purification). Each group represents pooled tumors from 5 different mice. Indicated P values were calculated by the Wilcoxon test.

Figure 6

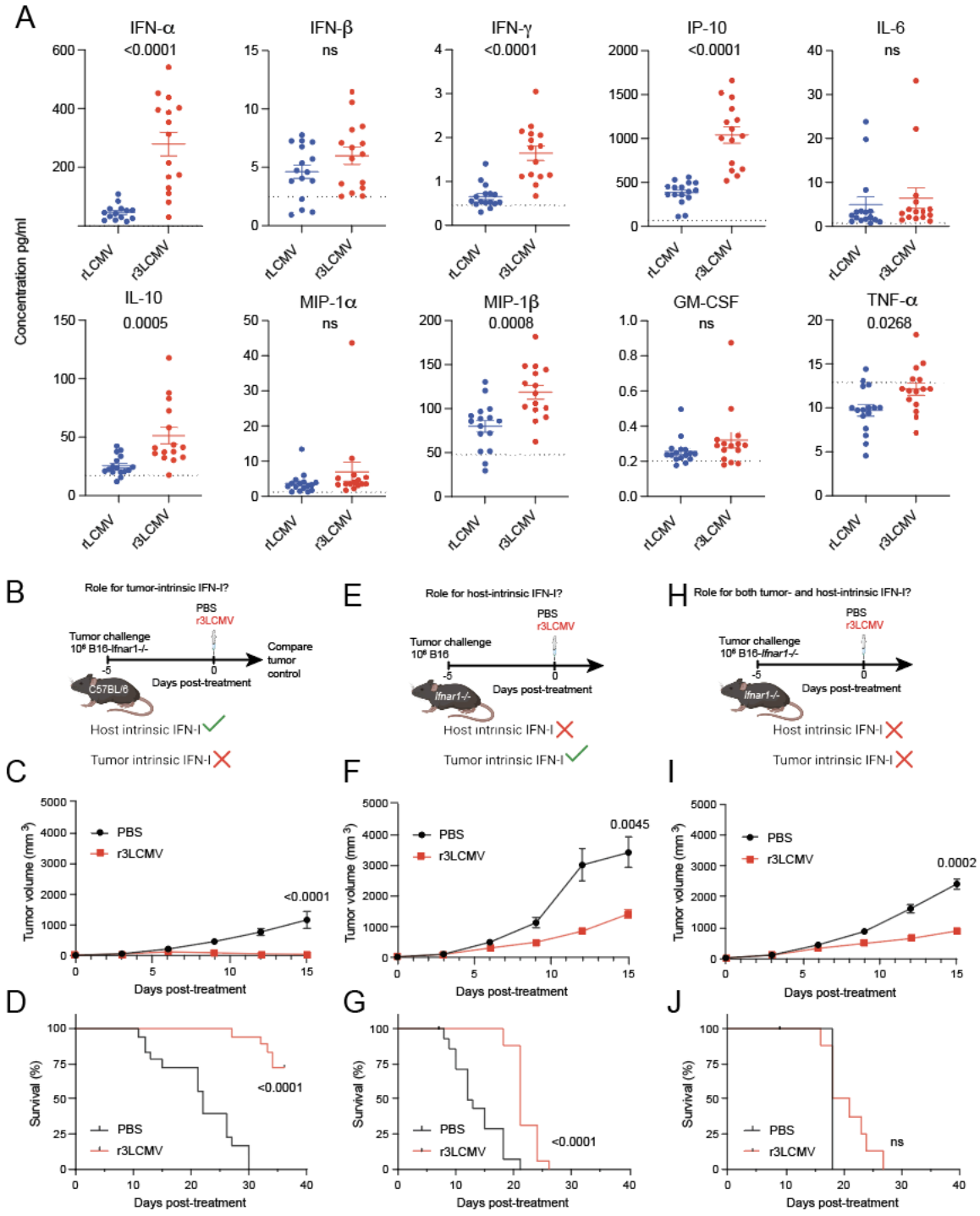

Figure 6. **Confirmatory mechanistic studies corroborate a role for IFN-I**. (**A**) Cytokine responses at day 1 post-treatment. Dashed lines represent naïve levels. (**B-D**) Effect of r3LCMV vectors on B16 *Ifnar1*-/- melanoma. (**B**) Experiment outline for evaluating the

role of tumor-intrinsic IFN-I. (**C**) Tumor control. (**D**) Survival. (**E-G**) Effect of r3LCMV vectors on *Ifnar1*-/- mice. (**E**) Experiment outline for evaluating the role of host-intrinsic IFN-I. (**F**) Tumor control. (**G**) Survival. (**H-J**) Effect of r3LCMV vectors on B16 *Ifnar1*-/- melanoma in *Ifnar1*-/- mice. (**H**) Experiment outline for evaluating the combined role of tumor-intrinsic and host-intrinsic IFN-I. (**I**) Tumor control. (**J**) Survival. Data from panel A are pooled from 3 experiments (one experiment with n=5 per group, another with n=5 per group, and another with n=5-6 per group). Data from panels B-G are pooled from 2 experiments (one experiment with n=8-9 per group, and another with n=8-10 per group). Data from panels H-J are pooled from 2 experiments (n=4-5 per group). Error bar represents SEM. Indicated P values were calculated by the Mann–Whitney test, or log rank test when comparing survival.

Figure 7

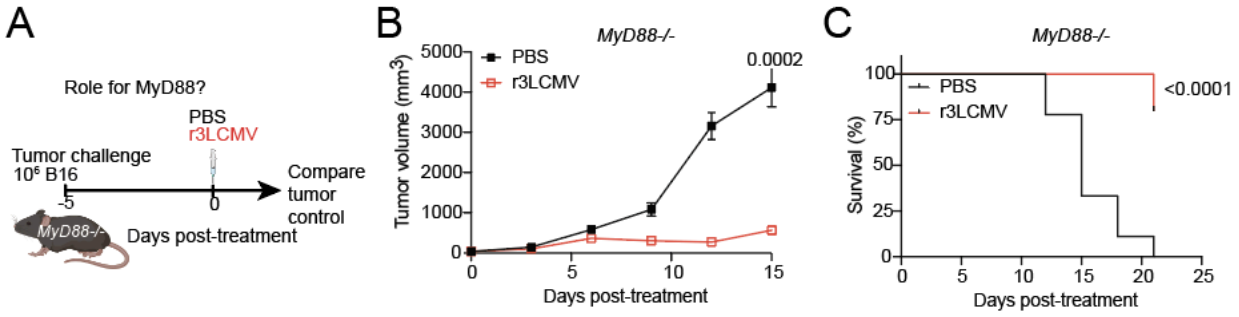

Figure 7. r3LCMV therapy improves tumor control in *MyD88*-/- mice. (**A**) Experiment outline. The set up was similar to Figure 1, but using *MyD88*-/- mice instead of wild-type mice. (**B**) Tumor control. (**C**) Survival. Data are pooled from 2 experiments (n=4-5 per group/experiment). Error bar represents SEM. Indicated P values were calculated by the Mann–Whitney test, or log rank test when comparing survival.

Figure 8

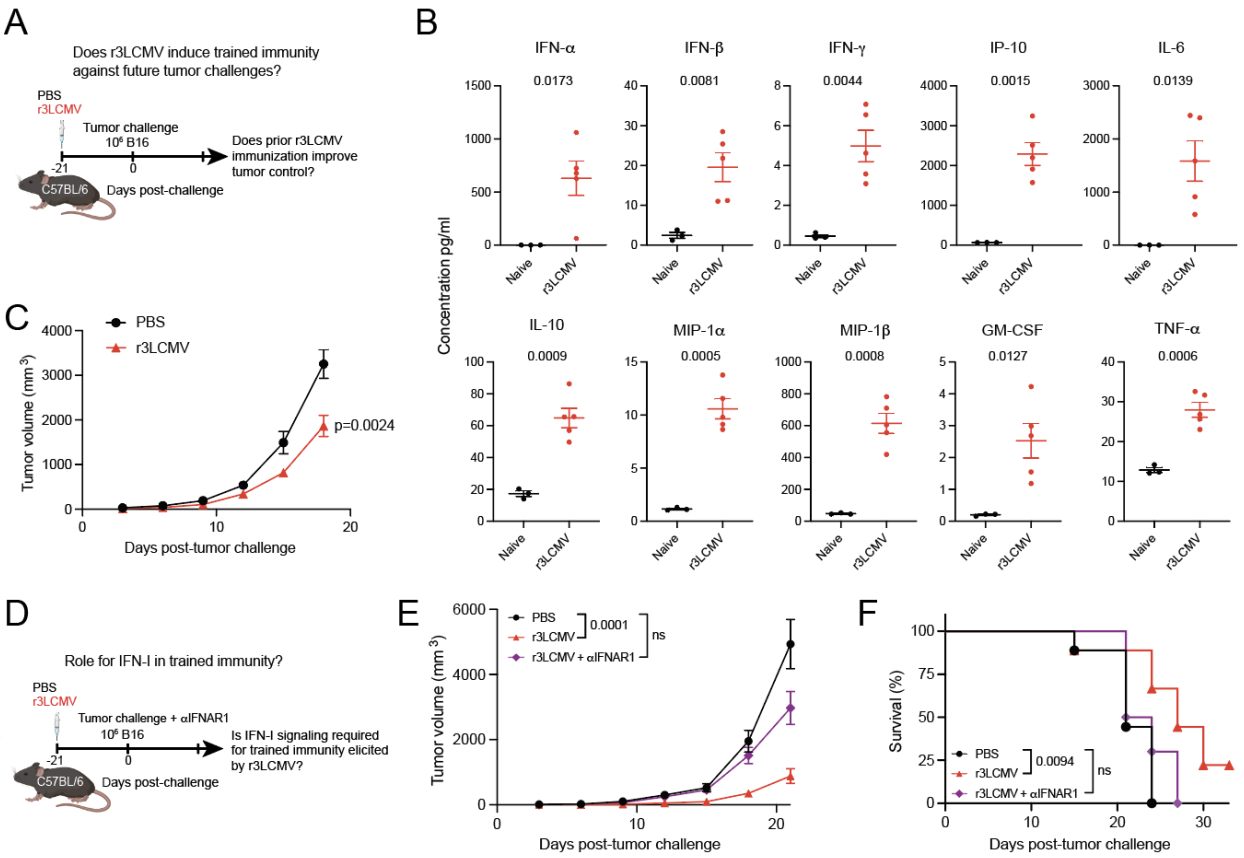

Figure 8. Prior treatment with r3LCMV renders mice more resistant to tumor challenges. We tested whether mice that had previously been injected with r3LCMV were protected upon subsequent tumor challenges. (**A**) Experiment outline to evaluate the effect of prior r3LCMV treatment on subsequent tumor challenges (trained immunity). (**B**) Cytokine responses at day 1 post-r3LCMV treatment. (**C**) Tumor control. (**D**) The experiment in panel A was repeated, but mice were treated with IFNAR1 blocking antibodies at the time of tumor challenge (see Materials and Methods) to examine the role of IFN-I signaling. (**E**) Tumor control in the context of IFNAR1 blockade. (**F**) Survival in the context of IFNAR1 blockade. Cytokine data from panel B are from 1 experiment with n=5 mice (naïve mice are shown as controls); experiment was repeated with similar results. Data from panel C are from 2 experiments, n=13 per group. Data from panel D-F

are from 2 experiments (n=4-5 per group). Error bar represents SEM. Indicated P values in cytokine plots were calculated by the Welch’s t test. Indicated P values in the tumor volume plots were calculated by the Mann–Whitney test, or Kruskal-Wallis (Dunn's multiple comparison) test when comparing more than 2 groups. Indicated P values in the survival plot were calculated by the log rank test.